Deciphering the Influence of Short-Range Electronic Couplings on Optical Properties of Molecular Dimers: Application to "Special Pairs" in Photosynthesis

Mohamed El-Amine Madjet, Frank Müh, and Thomas Renger*

Freie Universität Berlin, Institut für Chemie und Biochemie (Kristallographie), Fabeckstrasse 36a, D-14195 Berlin, Germany

Received: June 26, 2009; Revised Manuscript Received: July 24, 2009

The excited states of chromophore dimers are, in general, delocalized, and the transition energies and transition dipoles are different from those of the monomers. The intermolecular interaction that is responsible for these effects has two contributions: Förster-type Coulomb coupling and a short-range coupling, which depends on the intermolecular overlap of electronic wave functions. The latter contains the Dexter-type exchange coupling and the coupling of excited states to intermolecular charge-transfer (CT) states. Recently, we developed a method (TrEsp) for an accurate and numerically efficient calculation of the Förster-type Coulomb part (Madjet et al. *J. Phys. Chem. B* **2006**, *110*, 17268). Here, we combine the latter with quantum chemical calculations to evaluate the short-range contribution, extending a method developed earlier by Scholes et al. (*J. Phys. Chem. B* **1999**, *103*, 2543). An effective two-state model is used, which relates the transition energies and transition dipole moments obtained by quantum chemical calculations of the monomers to those calculated for the dimer. From this relation, the short-range excitonic coupling and effective shifts of the local transition energies due to the coupling to intermolecular CT states can be inferred including a consistency check to evaluate quantum chemical methods that differ in the treatment of electron correlation. The method is applied to the special pairs of the reaction centers of purple bacteria (bRC) and photosystem I (PSI). We find that the short-range coupling represents the dominant contribution to the total excitonic coupling in both special pairs (80% in PSI and 70% in the bRC) and exhibits a monoexponential dependence on the distance between the π-planes of the pigments with an attenuation factor of 2.8 $Å^{-1}$. We obtain significant red-shifts of the local transition energies, which show a biexponential distance dependence with one attenuation factor being 2.8 $Å^{-1}$ and another factor being in the range 0.3−0.7 $Å^{-1}$ for PSI and 0.8−0.9 $Å^{-1}$ for bRC. Both effects of the short-range coupling determine the excitation energy sink in the reaction centers at the special pairs.

Downloaded via UNIV OF OKLAHOMA on June 24, 2018 at 17:58:37 (UTC).
See https://pubs.acs.org/sharingguidelines for options on how to legitimately share published articles.

I. Introduction

Excitation energy transfer is a process in which the electronic excitation energy of a dye molecule is transferred to another molecule by a radiationless mechanism. This type of energy transfer is of particular importance in photosynthesis,[1–3] where solar photons are absorbed by light-harvesting complexes.[4–7] These pigment−protein complexes (PPCs) contain a large number (on the order of 20−300) of chlorophyll cofactors,[3,8,9] which interact with each other and with the protein scaffold such as to create excitation energy pathways. The excitation energy is transferred along these pathways to a specialized subset of six pigments forming the reaction center, where it drives the formation of a charge-separated state, initiating the conversion of light energy into chemical energy.[3,10–12]

A prerequisite for excitation energy transfer is the existence of an electronic matrix element V that connects the initial state $|D^*A\rangle$, in which the donor molecule D is excited and the acceptor A is in its ground state, with the final state $|DA^*\rangle$, in which only A is excited. This matrix element V, that is termed excitonic coupling, can be partitioned into a long-range contribution V_{LR} and a short-range contribution V_{SR}.

Whereas V_{LR} describes the Coulomb interaction between the transition densities of the optical transitions on molecules D and A[13,14] and exhibits an R^{-3} distance dependence for large intermolecular distances R, V_{SR} depends on the intermolecular overlap of the electronic wave functions, which results in an exponential distance dependence. As a consequence, V_{SR} can be neglected at larger distances. It is this "long-range limit" for which Förster developed his theory of resonance energy transfer.[15] The Förster coupling can be envisaged as a concerted excitation−deexcitation process, in which only energy but no electrons are exchanged between molecules, as illustrated within the framework of a simple frontier orbital model in the left part of Figure 1A. Here, $V_{LR} \approx J_{ex}$, where J_{ex} is the Coulomb integral involving the highest occupied molecular orbitals (HOMOs) and lowest unoccupied molecular orbitals (LUMOs) of the two molecules (as discussed in the Supporting Information). Förster applied a dipole approximation to estimate V_{LR}, which for many antenna systems describes the major part of the excitonic coupling. This type of coupling can already be large enough to cause significant delocalization of excited states. The prototype example for such a situation is the Fenna−Matthews−Olson (FMO) protein, which has been used as a model system in numerous experimental and theoretical studies (for a recent review, see ref 16).

The dipole approximation becomes invalid for small intermolecular distances, where quantum chemical methods have to be used to obtain the transition densities of the interacting molecules. We have recently developed an accurate and numerically efficient method for the calculation of V_{LR}, that combines the simplicity of semiempirical transition monopole approaches[17–20] with the accuracy of the *ab initio* transition density cube (TDC) method.[21] In this TrEsp (transition charges from electrostatic potential) method,[14] atom-centered transition

10.1021/jp906009j CCC: $40.75 © 2009 American Chemical Society
Published on Web 08/21/2009

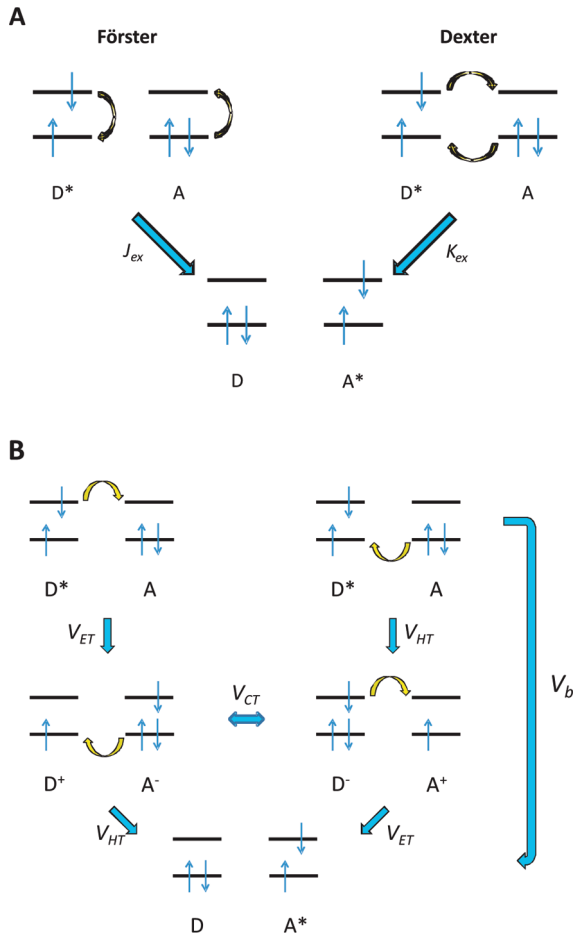

Figure 1. Illustration of different mechanisms to transfer an excitation from a donor molecule D to an acceptor molecule A. In the Förster mechanism (left part of panel A), the excitation energy is transferred without exchanging electrons between the molecules. The Dexter transfer (right part of panel A) considers a simultaneous exchange of two electrons. In the superexchange mechanism (panel B), two charge-transfer states form a bridge that connects the two local excited states via two sequential one-electron-transfer events.

charges are obtained from a fit of the three-dimensional electrostatic potential of the *ab initio* transition density of a molecule. V_{LR} is calculated from the Coulomb coupling between the transition charges of the two molecules.

In addition to corrections of the dipole approximation for V_{LR}, overlap dependent short-range contributions become important at small intermolecular distances. The exchange contributions to the excitonic coupling V were first studied by Dexter.[22] The Dexter-type coupling K_{ex} can be thought of as a double electron transfer between the LUMOs and HOMOs of the two molecules (Figure 1A, right), which is made possible by the intermolecular wave function overlap. However, as noted by Harcourt, Scholes, and Ghiggino,[23,24] the situation is more complex, because the overlap also allows for electron transfer (ET) or hole transfer (HT), thus coupling charge-transfer (CT) states to the exciton states (Figure 1B). The CT states form a bridge that couples the two localized excited states by a superexchange-type matrix element V_b, depending on the matrix elements for the individual hole- and electron-transfer events V_{HT} and V_{ET}, respectively, and on the energy gap between the localized excited states and the CT states. In general, the coupling to the CT bridges will not only lead to a change of V but will also shift the local transition energies of the two molecules (see section II).

The direct calculation of electron-transfer matrix elements is a nontrivial task.[13,20,25,26] Scholes et al.[27] developed a method to determine V_{SR} that circumvents such a direct calculation. In this method, the quantum chemically calculated transition energies of the separate monomers are related to those of the dimer using an effective two-state Hamiltonian. The off-diagonal element of the Hamiltonian represents an effective excitonic coupling, while its diagonal elements are effective local transition energies. The former can be decomposed into a long-range and a short-range excitonic coupling V_{LR} and V_{SR}, respectively, by an independent calculation of V_{LR}. The shift of the effective local transition energies with respect to the original site energies was assumed to be the same for both monomers,[27] implying that the CT states mix equally with the local excited states of the monomers, and assuming also a symmetric influence of the intermolecular charge density Coulomb coupling. The present method allows one to take into account different shifts of the local transition energies and to distinguish between long-range and short-range site energy shifts. To extract these quantities, it is necessary to use the information about the monomer and dimer transition dipole moments obtained from the quantum chemical calculations. This information also allows one to check the effective two-state approach for consistency.

As shown by Scholes et al.,[27] the short-range coupling between neighboring bacteriochlorophyll *a* molecules in the B850 ring of the peripheral light-harvesting complex LH2 of purple bacteria amounts to about 20% of the Coulomb part. Another class of systems, where the short-range coupling is expected to be important, is represented by the reaction centers of purple bacteria (bRC)[28] and photosystem I (PSI),[29] which contain a strongly coupled (bacterio)chlorophyll dimer known as a special pair. Since the interpigment distances in these special pairs are even smaller than those for neighboring pigments in the LH2 complex, it can be expected that the short-range contribution is larger.

The bRC was investigated by Warshel and Parson,[20] using a semiempirical method that includes a transition monopole treatment of the coupling between the transition densities of local excited states and also the coupling between local excited and CT states. It was found that the latter type of coupling (described above by V_{ET} and V_{HT}) is larger in magnitude than the coupling of transition densities and is responsible for the strong red-shift of the low-energy absorbance band of the special pair. In the present *ab initio* treatment, we arrive at the same conclusion and show that it holds also for the special pair in PSI. A conceptual difference of the present method with respect to that of Warshel and Parson is the calculation of effective short-range site energy shifts and excitonic couplings that can be directly incorporated into the diagonal and off-diagonal elements of standard multichromophore exciton Hamiltonians. In the past, these quantities were often treated as fit parameters in the calculations of optical spectra.[30–36] Here, we aim at a direct calculation.

This work is organized as follows: In part II, we present the theory behind our effective two-state approach. The computational methods are briefly described in part III, and the approach is applied in part IV to the special pairs of bRC and PSI. A discussion of the results is presented in part V, and conclusions are drawn in part VI. Additional details are given in Appendices A, B, and C and the Supporting Information.

II. Theory

A. The Effective Two-State Hamiltonian. In order to extract the influence of the CT states on the exciton states from quantum chemical calculations without explicit calculation of the short-range coupling matrix elements, we introduce an effective two-state Hamiltonian

$$\tilde{\mathbf{H}}_2 = \begin{pmatrix} \tilde{\varepsilon}_1 & \tilde{V} \\ \tilde{V} & \tilde{\varepsilon}_2 \end{pmatrix} \quad (1)$$

where the two basis states $|\tilde{\Psi}_1\rangle$ and $|\tilde{\Psi}_2\rangle$ are mixed local excited/CT states of the form

$$|\tilde{\Psi}_1\rangle = N_1^{-1}(a|\Psi_1\rangle + \sum_k \alpha_k|\Psi_k\rangle) \quad (2)$$

and

$$|\tilde{\Psi}_2\rangle = N_2^{-1}(b|\Psi_2\rangle + \sum_k \beta_k|\Psi_k\rangle) \quad (3)$$

Here, $|\Psi_1\rangle = |D^*A\rangle$ and $|\Psi_2\rangle = |DA^*\rangle$ are local excited states resulting from excitation of the $S_0 \rightarrow S_1$ transitions of the two monomers D and A, respectively, and the $|\Psi_k\rangle$ denote intermolecular CT states. As an example, a four-state Hamiltonian that contains two charge-transfer states $|\Psi_3\rangle = |D^+A^-\rangle$ and $|\Psi_4\rangle = |D^-A^+\rangle$ which result from electron transfer between the HOMO of D and the LUMO of A and the HOMO of A and the LUMO of D, respectively, is shown in Appendix A. The normalization constants in eqs 2 and 3 are $N_1 = (a^2 + \sum_k \alpha_k^2)^{1/2}$ and $N_2 = (b^2 + \sum_k \beta_k^2)^{1/2}$. We consider situations in which the electron exchange coupling is small compared to the energy difference between the CT states and the local excited states. In this limit, it holds that $a > 0$ and $b > 0$.

To distinguish between the different contributions to the effective excitonic coupling $\tilde{V}$ and the effective local transition energies $\tilde{\varepsilon}_i$, we write the matrix elements of $\tilde{\mathbf{H}}_2$ in eq 1 as

$$\tilde{V} = V_{LR} + V_{SR} \quad (4)$$

and

$$\tilde{\varepsilon}_i = \varepsilon_i^{(0)} + \lambda_i^{(LR)} - \lambda_i^{(SR)} \quad (5)$$

where $V_{LR} = J_{ex}$ is the long-range Coulomb coupling between transition densities. The short-range coupling $V_{SR} = K_{ex} + V_b$ contains the Dexter exchange integral K_{ex} and a contribution V_b from the mixing with the CT states (Figure 1). The $\varepsilon_i^{(0)}$ are the monomer transition energies, $\lambda_i^{(LR)}$ the long-range site energy shifts resulting from the Coulomb coupling between the charge densities of the monomers, as discussed below, and $\lambda_i^{(SR)}$ the site energy shifts due to exchange couplings between the monomers and the mixing of local excited states with CT states. The different sign convention used for $\lambda_i^{(LR)}$ and $\lambda_i^{(SR)}$ in eq 5 was introduced because short-range site energy shifts are expected to lead to lower site energies, whereas long-range shifts have no preference.

While $\varepsilon_i^{(0)}$ and $\lambda_i^{(LR)}$ are obtained from quantum chemical calculations on the monomers and electrostatic calculations on the dimers, $\tilde{V}$ and $\lambda_i^{(SR)}$ are deduced by relating the results from the quantum chemical dimer calculations to those of the monomers. For this purpose, $\tilde{\mathbf{H}}_2$ is diagonalized, and the short-range quantities extracted. Details are given in Appendix B. The result is

$$\lambda_{1/2}^{(SR)} = \varepsilon_{1/2}^{(0)} + \lambda_{1/2}^{(LR)} - \frac{1}{2}(E_+ + E_-) \pm \frac{1}{2}(E_+ - E_-)\frac{Y^2 - 1}{Y^2 + 1} \quad (6)$$

$$V_{SR} = (E_+ - E_-)\frac{Y}{1 + Y^2} - V_{LR} \quad (7)$$

where E_+ and E_- are the high- and low-energy eigenvalues, respectively, of $\tilde{\mathbf{H}}_2$, which we identify with the two lowest excitation energies of the dimer. The quantity Y is obtained from the transition dipole moments of the monomers, $\boldsymbol{\mu}_{0i}$ ($i = 1, 2$), and that of the dimer, $\boldsymbol{\mu}_{0\pm}$, assuming that the CT states are optically dark (see Appendix B), as

$$Y = -f\,\frac{g_1(\boldsymbol{\mu}_{0-})}{g_1(\boldsymbol{\mu}_{0+})} = Y_a \quad (8)$$

Y also fulfills the following equation:

$$Y = f\,\frac{g_2(\boldsymbol{\mu}_{0+})}{g_2(\boldsymbol{\mu}_{0-})} = Y_b \quad (9)$$

The quantities g_1, g_2 and f in eqs 8 and 9 are given as

$$g_1(\boldsymbol{\mu}) = (\boldsymbol{\mu}\cdot\boldsymbol{\mu}_{01})(\boldsymbol{\mu}_{02})^2 - (\boldsymbol{\mu}\cdot\boldsymbol{\mu}_{02})(\boldsymbol{\mu}_{01}\cdot\boldsymbol{\mu}_{02}) \quad (10)$$

$$g_2(\boldsymbol{\mu}) = (\boldsymbol{\mu}\cdot\boldsymbol{\mu}_{02})(\boldsymbol{\mu}_{01})^2 - (\boldsymbol{\mu}\cdot\boldsymbol{\mu}_{01})(\boldsymbol{\mu}_{01}\cdot\boldsymbol{\mu}_{02}) \quad (11)$$

and

$$f = 1 \quad \text{if} \quad g_1(\boldsymbol{\mu}_{0+})g_2(\boldsymbol{\mu}_{0-}) > 0, \quad \text{and} \quad f = -1 \quad \text{otherwise} \quad (12)$$

The equality of Y_a (eq 8) and Y_b (eq 9) will be used as a consistency check of our method. The monomer transition dipole moments $\boldsymbol{\mu}_{0i}$ and the dimer transition dipole moments $\boldsymbol{\mu}_{0\pm}$, that determine Y, are obtained from quantum chemical monomer and dimer calculations, respectively (see below). Differences between Y_a and Y_b can be expected, if the low-energy localized excited states significantly mix, besides the CT states, with other states that have a nonvanishing transition dipole moment. In this case, eqs B8 and B9 in Appendix B would become invalid. Consequently, the outcome of the quantum chemical dimer calculation could not be described by the effective two-state Hamiltonian in eq 1. Finally, we note that the neglect of overlap between states $\tilde{\Psi}_1$ and $\tilde{\Psi}_2$ (eqs 2 and 3) in the diagonalization of the effective two-state Hamiltonian (eq B1) can be justified, as shown in the Supporting Information.

B. Extraction of Excitonic Coupling and Site Energy Shifts. The quantum chemical calculations on the monomers not only yield the monomer transition dipole moments $\boldsymbol{\mu}_{0i}$ and transition energies $\varepsilon_i^{(0)}$ but, in addition, the electrostatic potential (ESP) of the charge density of the electronic ground state S_0 and the excited state S_1, and the ESP of the $S_0 \rightarrow S_1$ transition density. The ESP of these quantities is fitted by the ESP of atomic partial charges $q_I^{(C)}(k,l)$, as described in detail in ref 14. Here, I counts the nuclei of monomer C = D, A, while $k = l = 0$ for the ground state charge density, $k = l = 1$ for that of the excited state, and $k = 0$, $l = 1$ for the transition density.

Quantum chemical calculations of the dimer result in transition dipole moments $\boldsymbol{\mu}_{0\pm}$ and energies $E_\pm$ of the exciton states. The $Y_{a/b}$ values in eqs 8 and 9 are obtained from the monomer and dimer transition dipole moments (eqs 10−12). On the basis of these $Y_{a/b}$ values, the short-range excitonic coupling V_{SR} follows from eq 7, where the long-range part V_{LR} is calculated by using the TrEsp method:[14]

$$V_{LR} = \sum_{I,J} \frac{q_I^{(D)}(0,1) q_J^{(A)}(0,1)}{|\mathbf{R}_I^{(D)} - \mathbf{R}_J^{(A)}|} \tag{13}$$

Here, $\mathbf{R}_I^{(D)}$ and $\mathbf{R}_J^{(A)}$ are the coordinates of the Ith atom of monomer D and the Jth atom of monomer A.

The Coulomb (long-range) part V_{LR} of the total excitonic coupling in eq 4 depends on the TrEsp transition charges, as shown in eq 13. These charges usually overestimate the monomer transition dipole moments $\boldsymbol{\mu}_{0i}$. For consistency, they are used without change in the calculation of $V_{SR} = \tilde{V} - V_{LR}$.[27] In order to obtain a more realistic total coupling, that can be used to describe optical spectra of pigment−protein complexes, we correct the long-range coupling afterward in the following way:[27] The transition charges $q_I^{(C)}(0,1)$ of the monomers C = D, A in eq 13 are rescaled to yield a dipole moment magnitude μ_{eff} that takes into account the vacuum dipole strength, estimated from experimental data,[37] and includes local field and screening effects due to the polarizability of the protein in an effective way:

$$q_{I_{eff}}^{(C)}(0,1) = q_I^{(C)}(0,1) \frac{\mu_{eff}}{|\sum_J q_J^{(C)}(0,1)\mathbf{R}_J^{(C)}|} \tag{14}$$

Local field and screening effects of the Coulomb interaction between optical transition densities of the pigments were quantitatively investigated[38,39] in electrostatic calculations on the FMO protein, resulting in an effective dipole moment of μ_{eff} = 5.48 D for bacteriochlorophyll *a* (BChl*a*). This value will be used also in the present work. For chlorophyll *a* (Chl*a*), no such calculations have been performed yet. We assume that the same screening/local field factor for the Coulomb coupling of 0.8 as determined for BChl*a*[38,39] also applies to Chl*a*, resulting in an effective dipole moment of 4.10 D.

The total effective excitonic coupling $\tilde{V}_{eff}$ is then given by

$$\tilde{V}_{eff} = V_{SR} + V_{LR}^{(eff)} \tag{15}$$

where $V_{LR}^{(eff)}$ is the rescaled long-range part, obtained from eq 13 by replacing the transition charges by the rescaled quantities in eq 14. In applications of $\tilde{V}_{eff}$ to simulations of optical spectra of PPCs, it is implicitly assumed that effects of the protein matrix on V_{SR} can be neglected. Of course, the energies of CT states will be shifted in a dielectric environment. However, for the present superexchange mechanism, the exact energies of the bridge states may not be so crucial as long as their difference to the energies of the exciton states remains large compared to the respective coupling matrix elements.

According to eq 6, the short-range energy shift $\lambda_i^{(SR)}$ depends on the monomer transition energy $\varepsilon_i^{(0)}$ and the long-range site energy shift $\lambda_i^{(LR)}$. The latter describes the site energy shift due to the change in charge density coupling between the two monomers that occurs when monomer i is excited. It is obtained as[14]

$$\lambda_{1/2}^{(LR)} = \sum_{I,J} \frac{(q_I^{(D/A)}(1,1) - q_I^{(D/A)}(0,0)) q_J^{(A/D)}(0,0)}{|\mathbf{R}_I^{(D/A)} - \mathbf{R}_J^{(A/D)}|} \tag{16}$$

where the partial charges $q_I^{(C)}$ are obtained from the quantum chemical calculations on the monomers as described above. As in the case of the coupling $\tilde{V}$, there are two solutions for the values of λ_i obtained from Y_a or Y_b, which are used as a consistency check.

III. Computational Methods

Spatial coordinates of the BChl*a* dimer of the bRC from *Rhodobacter sphaeroides* and for the Chl*a* dimer of PSI from *Thermosynechococcus elongatus* were taken from PDB files 1AIJ[28] and 1JB0,[29] respectively. We note that the special pair of PSI is actually a Chl*a*/Chl*a*′ heterodimer, which is taken into account in our calculations. The originally incorrect coordinates for Chl*a*′ were corrected (Norbert Krauβ, private communication) and are given in the Supporting Information. Hydrogen atoms were added with the help of CHARMM.[40,41] For geometry optimization, the program Jaguar[42] was used applying density functional theory (DFT) with the B3LYP exchange-correlation (XC) functional and a 6-31G** basis set. The geometry optimization was performed with constraining of the torsional angles to their values in the crystal structure to take into account the different conformations of the pigments and, in this way, part of the influence of the protein environment. Electronic structure calculations were carried out with Q-Chem[43] based on the optimized geometries. Excited states were calculated using either the Hartree−Fock approximation with configuration interaction of single excitations (HF-CIS) or time-dependent density functional theory (TDDFT) with different exchange-correlation (XC) functionals: the standard B3LYP XC functional containing 20% HF exchange, the Becke-Half-and-Half-LYP (BHHLYP) XC functional containing 50% HF exchange, and the newly defined B65LYP XC functional that contains 65% HF exchange. The total exchange and correlation energies in B3LYP, BHHLYP, and B65LYP are given by

$$\begin{aligned} E_{xc}^{B3LYP} &= 0.20E_x^{HF} + 0.80E_x^{LSDA} + 0.72\Delta E_x^{B} + \\ &\qquad 0.81E_c^{LYP} + 0.19E_c^{VWN} \\ E_{xc}^{BHHLYP} &= 0.50E_x^{HF} + 0.50(E_x^{LSDA} + \Delta E_x^{B}) + E_c^{LYP} \\ E_{xc}^{B65LYP} &= 0.65E_x^{HF} + 0.35(E_x^{LSDA} + \Delta E_x^{B}) + E_c^{LYP} \end{aligned} \tag{17}$$

where E_x^{HF}, E_x^{LSDA}, ΔE_x^{B}, E_c^{LYP}, and E_c^{VWN} represent the HF exchange,[44] the Slater local exchange energy,[47] Becke's 1988 nonlocal gradient correction to the local spin density approximation for exchange,[45] the Lee, Yang, and Parr correlation energy,[46] and the Vosko−Wilk−Nusair local correlation functional,[48] respectively.

Fits of electrostatic potentials by atomic partial charges for calculations of V_{LR} (eq 13) and $\lambda_i^{(LR)}$ (eq 16) were done with CHELP-BOW.[49] More details are given in ref 14.

IV. Results

As a first consistency check of our quantum chemical calculations, we investigated how the transition energies obtained from the dimer calculations change as a function of the intermolecular distance. For this purpose, one pigment was translated along the normal on its tetrapyrrole plane away from

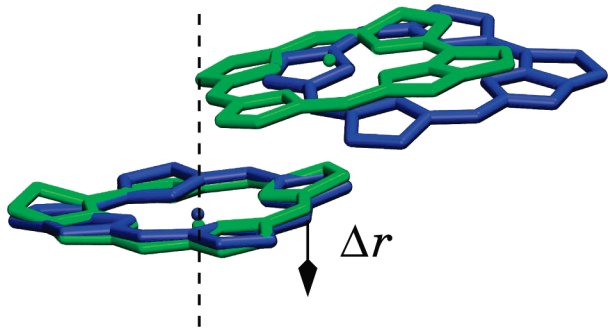

Figure 2. Overlay of the tetrapyrrole skeletons of the special pairs of bRC of *Rb. sphaeroides*[28] (blue) and PSI of *T. elongatus*[29] (green) viewed approximately along the π-plane. The arrow indicates a translation of one pigment along the normal on its plane (dashed line) away from the other pigment by a distance Δr. This translation is used to infer the distance dependence of the short-range effects. The overlay was obtained from a minimization of the mean-square deviation in positions of equivalent atoms of one dimer half of the two molecule pairs using the program VMD.[74]

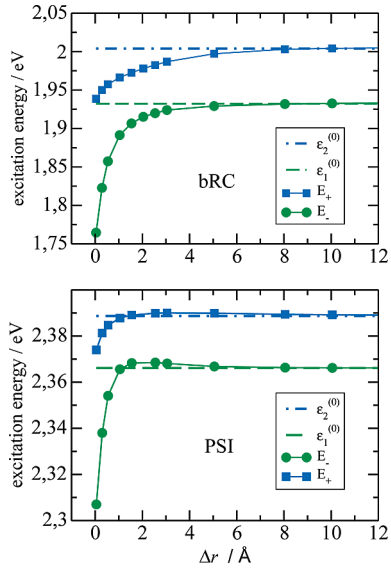

Figure 3. Dependence of dimer excitation energies E_+ and E_- on the displacement Δr (Figure 2) for the special pairs of the bRC (top panel) and PSI (bottom panel) obtained with HF-CIS and TDDFT/BHHLYP, respectively. The displacement $\Delta r = 0$ refers to a native interplane distance of about 3.5 Å for both structures. The excitation energies of the monomers $\varepsilon_1^{(0)}$ and $\varepsilon_2^{(0)}$ obtained with the same quantum chemical methods are shown for comparison (horizontal lines).

the other pigment, as indicated in Figure 2. The resulting two lowest excitation energies of the dimer are compared in Figure 3 with the two low excitation energies obtained for the monomers, where the same quantum chemical method was used for both, monomers and dimers (HF/CIS for bRC and TDDFT/BHHLYP for PSI). The dimer transition energies approach those calculated for the monomers at large distances, showing the size consistency of the quantum chemical calculations. Note that the monomer transition energies of the two dimer halves are not equal, even in vacuum, because of conformational differences between the two monomers that originate from the crystal structure and are a consequence of the pigment−protein interaction (Figure 2). The differences between monomer and dimer transition energies will be used below to infer the short-range effects.

At short distances, a strong decrease of the dimer transition energies in both reaction centers is found. There is a range of intermediate interplane distances (5−8 Å, corresponding to displacements Δr of 1.5−4.5 Å), for which the dimer transition energies are larger than those of the monomers in PSI but not in bRC. This effect is due to the Coulomb coupling between the charge densities of the monomers, as will be shown further below.

TABLE 1: Short-Range (SR) and Long-Range (LR) Couplings (V) and Site Energy Shifts (λ) in Units of cm^{-1} Calculated with Four Different Quantum Chemical Methods for the Special Pair in the bRC of *Rb. sphaeroides*[a]

	B3LYP	BHHLYP	B65LYP	CIS
Y_a	24.75	12.31	1.65	**1.43**
Y_b	4.63	−0.62	1.17	**1.04**
$V_{SR}(Y_a)$	−186	−191	464	**269**
$V_{SR}(Y_b)$	−108	−857	553	**311**
$\Delta V_{SR}/\bar{V}_{SR}$	53%	127%	18%	**15%**
$V_{LR}^{(eff)}$	85	102	110	128
$\lambda_1^{(SR)}(Y_a)$	169	2080	1051	**871**
$\lambda_1^{(SR)}(Y_b)$	148	1182	778	**656**
$\lambda_2^{(SR)}(Y_a)$	6	1486	687	**647**
$\lambda_2^{(SR)}(Y_b)$	26	2384	960	**862**
$\Delta\lambda_{SR}/\bar{\lambda}_{SR}$	71%	47%	32%	**28%**
$\lambda_1^{(LR)}$	39	−169	52	−19
$\lambda_2^{(LR)}$	−134	−116	−131	−343

[a] The two solutions of Y, Y_a (eq 8), and Y_b (eq 9), are used to calculate relative errors $\Delta V_{SR}/\bar{V}_{SR}$ (eq 18) and $\Delta\lambda_{SR}/\bar{\lambda}_{SR}$ (eqs 19 and 20). The SR results obtained with HF/CIS (numbers in bold) have the smallest relative errors.

TABLE 2: Short-Range (SR) and Long-Range (LR) Couplings (V) and Site Energy Shifts (λ) in Units of cm^{-1} Claculated with Four Different Quantum Chemical Methods for the Special Pair in PSI of *T. elongatus*[a]

	B3LYP	BHHLYP	B65LYP	CIS
Y_a	6.64	**1.38**	1.92	2.59
Y_b	−0.47	**1.10**	1.36	1.78
$V_{SR}(Y_a)$	50	**179**	76	9
$V_{SR}(Y_b)$	−204	**192**	103	41
$\Delta V_{SR}/\bar{V}_{SR}$	331%	**7%**	31%	128%
$V_{LR}^{(eff)}$	11	36	40	46
$\lambda_1^{(SR)}(Y_a)$	−40	**455**	306	183
$\lambda_1^{(SR)}(Y_b)$	−418	**395**	250	145
$\lambda_2^{(SR)}(Y_a)$	−244	**469**	319	112
$\lambda_2^{(SR)}(Y_b)$	134	**529**	375	151
$\Delta\lambda_{SR}/\bar{\lambda}_{SR}$	19%	**13%**	18%	27%
$\lambda_1^{(LR)}$	177	164	123	161
$\lambda_2^{(LR)}$	241	165	195	173

[a] The two solutions of Y, Y_a (eq 8) and Y_b (eq 9), are used to calculate relative errors $\Delta V_{SR}/\bar{V}_{SR}$ (eq 18) and $\Delta\lambda_{SR}/\bar{\lambda}_{SR}$ (eqs 19 and 20). The SR results obtained with TDDFT/BHHLYP (numbers in bold) have the smallest relative errors.

The short-range couplings V_{SR} and site energy shifts $\lambda_i^{(SR)}$ extracted with our method for the special pairs of bRC and PSI at the native intermolecular distance (3.5 Å, $\Delta r = 0$) are shown in Tables 1 and 2. Different quantum chemical methods were applied. As discussed above, the difference between short-range coupling values and site energy shifts obtained for Y_a and Y_b is a measure of the consistency of the result. We introduce a relative error

$$\frac{\Delta V_{SR}}{\bar{V}_{SR}} = 2\frac{V_{SR}(Y_a) - V_{SR}(Y_b)}{V_{SR}(Y_a) + V_{SR}(Y_b)} \qquad (18)$$

of the short-range coupling. For the short-range site energy shifts, we have to consider the following two cases: if ($|Y_a| < 1$ and $|Y_b| < 1$) or ($|Y_a| > 1$ and $|Y_b| > 1$),

$$\frac{\Delta\lambda_{SR}}{\bar{\lambda}_{SR}} = \frac{|\lambda_1^{(SR)}(Y_a) - \lambda_1^{(SR)}(Y_b)|}{\lambda_1^{(SR)}(Y_a) + \lambda_1^{(SR)}(Y_b)} + \frac{|\lambda_2^{(SR)}(Y_a) - \lambda_2^{(SR)}(Y_b)|}{\lambda_2^{(SR)}(Y_a) + \lambda_2^{(SR)}(Y_b)} \quad (19)$$

and if ($|Y_a| > 1$ and $|Y_b| < 1$) or ($|Y_a| < 1$ and $|Y_b| > 1$),

$$\frac{\Delta\lambda_{SR}}{\bar{\lambda}_{SR}} = \frac{|\lambda_1^{(SR)}(Y_a) - (\lambda_2^{(SR)}(Y_b) + \delta\theta)|}{\lambda_1^{(SR)}(Y_a) + \lambda_2^{(SR)}(Y_b) + \delta\theta} + \frac{|\lambda_1^{(SR)}(Y_b) - (\lambda_2^{(SR)}(Y_a) + \delta\theta)|}{\lambda_1^{(SR)}(Y_b) + \lambda_2^{(SR)}(Y_a) + \delta\theta} \quad (20)$$

where $\delta\theta = \varepsilon_2^{(0)} + \lambda_2^{(LR)} - \varepsilon_1^{(0)} - \lambda_1^{(LR)}$. Equation 20 takes into account the existence of two solutions that differ in the relative weight of the two monomers in the exciton states of the dimer, as discussed in detail in Appendix C.

In the case of bRC of *Rb. sphaeroides* (Table 1), the smallest relative errors are obtained for the HF/CIS method. The TDDFT methods with B3LYP and BHHLYP XC-functional yield total excitonic couplings $\tilde{V}$ with an inverted sign. This sign inversion would redistribute the oscillator strength to the high-energy exciton state of the dimer, in contrast to the experimental observation.[50] The relative errors for B3LYP and BHHLYP XC functionals are also significantly higher than those of the HF/CIS method. In contrast, the relative errors for the B65LYP XC functional are only slightly larger than those of HF/CIS and the results are qualitatively similar.

In the case of the special pair in PSI, the smallest relative errors are obtained with TDDFT/BHHLYP (Table 2). The couplings and site energy shifts are about half in magnitude compared to the values obtained for bRC. Interestingly, the charge density coupling leads to a symmetric blue-shift ($\lambda_1^{(LR)} \approx \lambda_2^{(LR)}$) in the case of PSI and to an asymmetric red-shift ($|\lambda_1^{(LR)}| < |\lambda_2^{(LR)}|$) for the bRC special pair.

The distance dependence of the short- and long-range excitonic coupling in the two reaction centers is shown in Figure 4. As expected, the short-range part $\bar{V}_{SR} = (V_{SR}(Y_a) + V_{SR}(Y_b))/2$ decays rapidly with increasing distance. At an interplane distance of 5 Å (corresponding to $\Delta r = 1.5$ Å), it is practically zero. The long-range contribution $V_{LR}^{(eff)}$ switches sign and decays with the third inverse power of the distance, as expected for a dipole−dipole interaction. The dependence of $\bar{V}_{SR}$ on the displacement Δr (Figure 2) can be well described by a monoexponential function

$$\bar{V}_{SR}(\Delta r) \propto e^{-\beta\Delta r} \quad (21)$$

with an attenuation factor of $\beta \approx 2.8$ Å^{-1} (Figure 5). In the context of excitation energy transfer, the factor $1/\beta$ is sometimes called the effective Bohr radius.[51]

In contrast to $\bar{V}_{SR}$, the distance dependence of the two solutions ($Y_{a/b}$) of the short-range site energy shifts, $\lambda_1^{(SR)}$ and $\lambda_2^{(SR)}$, is not monoexponential (Figures 6 and 7). The simplest possible fit is obtained using a biexponential function

$$\lambda_i^{(SR)}(Y_j, \Delta r) = A_1(i,j)e^{-\beta_1(i,j)\Delta r} + A_2(i,j)e^{-\beta_2(i,j)\Delta r} \quad (i = 1,2; j = a,b) \quad (22)$$

where $\beta_2(i,j) = 2.8$ Å^{-1} equals the attenuation factor β of the excitonic coupling (Figure 5) and $\beta_1(i,j)$ is in the range

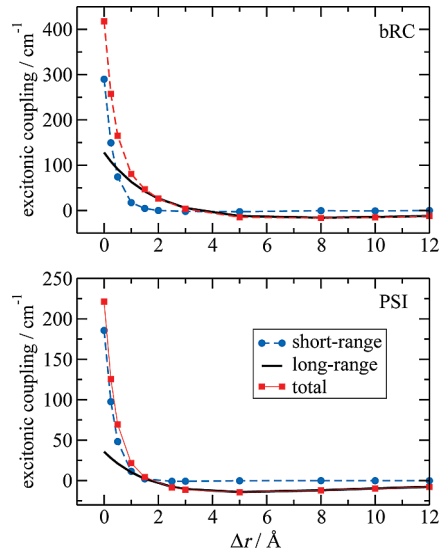

Figure 4. Dependence of the short-range excitonic coupling $\bar{V}_{SR} = (V_{SR}(Y_a) + V_{SR}(Y_b))/2$ (blue circles), the long-range excitonic coupling V_{LR}^{eff} (black line), and the total excitonic coupling $V_{eff} = \bar{V}_{SR} + V_{LR}^{(eff)}$ (red squares) on the displacement Δr (Figure 2) for the special pairs of bRC (top panel) and PSI (bottom panel). The displacement $\Delta r = 0$ refers to a native interplane distance of about 3.5 Å for both structures. These results were obtained with TDDFT/BHHLYP for PSI and HF/CIS for bRC.

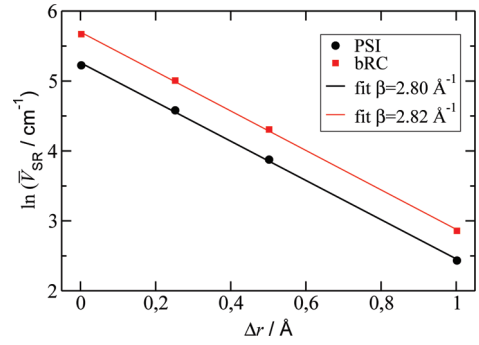

Figure 5. Natural logarithm of the short-range excitonic coupling $\bar{V}_{SR} = (V_{SR}(Y_a) + V_{SR}(Y_b))/2$ (Figure 4) as a function of the displacement Δr (Figure 2) for the special pairs of bRC and PSI. The displacement $\Delta r = 0$ refers to a native interplane distance of about 3.5 Å for both structures. The lines show linear regression fits resulting in the β values (eq 21) shown in the legend.

0.8−0.9 Å^{-1} for bRC and 0.3−0.7 Å^{-1} for PSI (Tables 3 and 4). Since Δr is the displacement with respect to the interplane distance found in the crystal structure (Figure 2), the sum of $A_1(i,j)$ and $A_2(i,j)$ resembles $\lambda_i^{(SR)}(Y_j)$ at the native distance (Tables 1 and 2). We note that β_2 in the present fits was fixed to the value of β. Allowing β_2 to vary results in very similar values.

V. Discussion

A. A Method for Estimating Short-Range Effects on Excitonic Couplings and Site Energy Shifts in Molecular Dimers. The present method extends the earlier approach of Scholes et al.[27] in three essential points: (i) A possible asymmetry of the dimer can be taken into account that may give rise to differences between $\lambda_1^{(SR)} + \lambda_1^{(LR)}$ and $\lambda_2^{(SR)} + \lambda_2^{(LR)}$, whereas $\lambda_1 = \lambda_2 = \lambda$ was assumed before.[27] (ii) The effect of the long-range Coulomb coupling on the site energy shifts described by $\lambda_i^{(LR)}$ is considered explicitly. In this way, it is

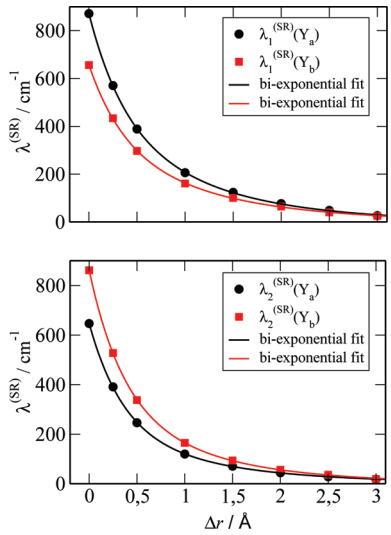

Figure 6. Dependence of the two solutions $\lambda_i^{(SR)}(Y_a)$ and $\lambda_i^{(SR)}(Y_b)$ of the short-range site energy shifts on the displacement Δr (Figure 2) for the special pair in bRC ($\Delta r = 0$ refers to a native interplane distance of about 3.5 Å). The lines show a biexponential fit (eq 22) using the parameters in Table 3. These results were obtained with HF/CIS.

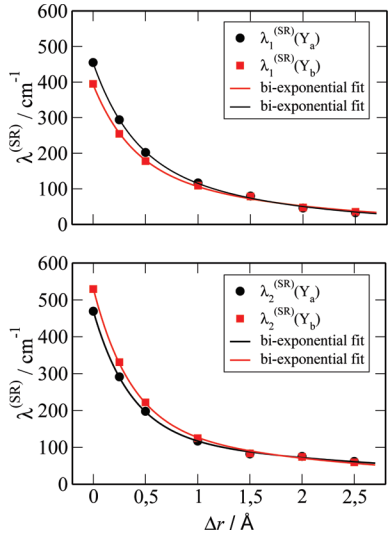

Figure 7. Dependence of the two solutions $\lambda_i^{(SR)}(Y_a)$ and $\lambda_i^{(SR)}(Y_b)$ of the short-range site energy shifts on the displacement Δr (Figure 2) for the special pair in PSI ($\Delta r = 0$ refers to a native interplane distance of about 3.5 Å). The lines show a biexponential fit (eq 22) using the parameters in Table 4. These results were obtained with TDDFT/BHHLYP.

TABLE 3: Parameters of eq 22 That Fit the Dependence of the Short-Range Site Energy Shifts $\lambda_{1/2}^{(SR)}(Y_{a/b})$ on the Displacement Δr in the Special Pair of bRC (Figure 6)

i	j	$A_1(i,j)$/cm^{-1}	$\beta_1(i,j)$/Å^{-1}	$A_2(i,j)$/cm^{-1}	$\beta_2(i)$/Å^{-1}
1	*a*	453	0.91	418	2.82
1	*b*	336	0.85	320	2.82
2	*a*	214	0.81	433	2.82
2	*b*	328	0.90	534	2.82

possible to extract the short-range contributions $\lambda_i^{(SR)}$ to the site energy shifts, whereas the previous parameter λ[27] contained a sum of both. (iii) The information about the quantum chemical transition dipole moments of the monomers and the dimer is used, which is a prerequisite for incorporating asymmetry in the model and provides a consistency check of the method.

TABLE 4: Parameters of eq 22 That Fit the Dependence of the Short-Range Site Energy Shifts $\lambda_{1/2}^{(SR)}(Y_{a/b})$ on the Displacement Δr in the Special Pair of PSI (Figure 7)

i	j	$A_1(i,j)$/cm^{-1}	$\beta_1(i,j)$/Å^{-1}	$A_2(i,j)$/cm^{-1}	$\beta_2(i,j)$/Å^{-1}
1	*a*	203	0.71	252	2.80
1	*b*	168	0.60	227	2.80
2	*a*	132	0.31	337	2.80
2	*b*	156	0.41	373	2.80

We note that application of the present method to the LH2 antenna system of purple bacteria, using the same HF/CIS quantum chemical method as in ref 27, yields a short-range excitonic coupling that amounts to about 25% of the total excitonic coupling, in good agreement with the value of 20% reported previously.[27] In addition, we obtain an asymmetric shift of the site energies by short-range effects that could not be obtained before (data will be presented elsewhere).

In the consistency check of the method, one has to distinguish two aspects: (i) the effective two-state approach relating monomer and dimer properties and (ii) the quantum chemical method. The approach (i) can be used in conjunction with different quantum chemical methods, and its reliability depends on the assumption that only optically dark states couple to the local excited states (eqs 2 and 3). The consistency is found to be strongly influenced by the quantum chemical methods (Tables 1 and 2) for reasons to be discussed below. The fact that some quantum chemical methods yield small relative errors lends support to the validity of the effective two-state approach for the present dimers. However, consistency alone does not guarantee that correct energy shifts and couplings are obtained. The final evaluation can only be performed by comparison with experiment. As shown below, the quantum chemical methods with the smallest relative error also yield best agreement with parameters extracted from fits of optical spectra, which is an encouraging result. When applying this method to other systems, one has to keep in mind that, if none of the applied functionals yields small relative errors, it is likely that the effective two-state approach is invalid and additional optical transitions have to be included explicitly in the analysis.

In the present application of the method to the special pairs of bRC and PSI, we find the smallest relative errors with TDDFT/BHHLYP for PSI and with HF/CIS for the bRC of *Rb. sphaeroides*. A well-known problem of TDDFT concerns the appearance of artificial excited states with low energies and partial CT character.[52] We also observe such states, in particular, when the B3LYP XC functional is used. One way to improve the accuracy of CT state energies is the use of Coulomb-attenuated XC functionals.[53–56] However, in the present cases, application of these functionals did not decrease the deviation between Y_a and Y_b below the smallest values obtained with BHHLYP for PSI and with HF/CIS for bRC (data not shown). The reason for this behavior is probably that the relevant CT states get involved here only via a superexchange mechanism. In a perturbation theory, the leading terms for site energy shifts and couplings scale with $v^2/\Delta E$, where v is an electron- or hole-transfer matrix element and ΔE is the energy difference between the local excited states and the CT states (see further below). As noted recently,[53–57] the TDDFT CT state energies are particularly erroneous for vanishing overlap between donor and acceptor wave functions. Since in this case v is approaching zero as well, the present calculations do not take notice of this error.

Thus, the following question remains: Why do the different quantum chemical methods perform so differently? As discussed

below, the intermolecular overlap of π-orbitals is stronger for bRC than for PSI. Our results seem to suggest that a larger overlap requires a larger amount of exact exchange to be included. It is certainly necessary to investigate a larger number of systems to draw definite conclusions about such a rule. The present class of hybrid functionals was designed to find an optimal description for each system by varying the amount of exact exchange between 20% for B3LYP and 65% for B65LYP (100% for HF/CIS) at the expense of dynamic correlation. We think that the balance between these two types of electron correlation is the key for a successful modeling.

It is well-known that HF/CIS overestimates transition dipole moments and transition energies.[58] Hence, at first glance, one might think that this fact causes a systematic error of our method scaling with the amount of exact exchange included. However, as long as the errors of the dimer quantities are similar to those of the monomers, the resulting errors for the extracted short-range quantities are much smaller, since only shifts in transition energies and dipole moments rather than absolute quantities are needed in the analysis. For example, if all of the quantum chemical transition dipole moments are off by the same factor with respect to the true values, the decisive value Y obtained from eqs 8−11 would not be effected by this absolute error. Note that there is an influence on the long-range excitonic coupling, which can, however, be corrected (eq 14).

The relatively minor differences between $\lambda_1^{(SR)}$ and $\lambda_2^{(SR)}$ in the two special pairs reflect the approximate C_2 symmetry of the dimer. The asymmetry in the Coulomb shift $\lambda_i^{(LR)}$ for bRC is due to the deviations from the C_2 symmetry of the substituents, in particular the 3-acetyl group, which seems to participate only weakly in the intermolecular short-range interactions. The different signs of $\lambda_i^{(LR)}$ obtained for bRC and PSI explain why, in PSI at intermediate intermolecular distances, the dimer transition energies are above those of the monomers (Figure 3). At these intermediate distances, the $\lambda_i^{(LR)}$ values (Supporting Information) are larger than the short-range site energy shifts $\lambda_1^{(SR)}$ and $\lambda_2^{(SR)}$ (Figure 7) and the long-range excitonic coupling $V_{LR}^{(eff)}$ (Table 2), resulting in a blue-shift of both excited dimer states with respect to the excited states of the isolated monomers. In the bRC, the $\lambda_i^{(LR)}$ are negative at all distances (see the Supporting Information) and therefore increase the red-shift of the dimer transition energies caused by $\lambda_i^{(SR)}$.

The present method allows one to distinguish between the effects of the short-range intermolecular couplings on the local transition energies and that on the excitonic couplings. In this way, it becomes possible to merge the present results with simple exciton theories by shifting the diagonal and off-diagonal elements of the exciton matrix accordingly. In fact, Scherer and Fischer[35] modified their exciton Hamiltonian in order to describe the low-temperature (4 K) bRC optical spectra of *Rb. sphaeroides*. The site energies were shifted by 600 cm^{-1} to the red with respect to the site energies of the monomeric BChl's, and the local excitonic coupling was adjusted to 680 cm^{-1}. These values are at least qualitatively similar to the $(\lambda_i^{(SR)}(Y_a) + \lambda_i^{(SR)}(Y_b))/2$ of 763 and 754 cm^{-1} ($i = 1, 2$) and the total excitonic coupling $V_{LR}^{(eff)} + (V_{SR}(Y_a) + V_{SR}(Y_b))/2$ of 418 cm^{-1} obtained here directly (Table 1). Mar and Gingras[36] uncovered the circular dichroism spectrum at 298 K of the bRC of *Ectothiorhodospira*. In their analysis, they shifted the site energies of the special pair by 350 cm^{-1} to the red of the monomeric BChl's and inferred an excitonic coupling of 340 cm^{-1}. Jordanides et al.[33] used an excitonic coupling of 395 cm^{-1} and a site energy shift of 600−700 cm^{-1} of the special pair pigments to model the room temperature absorbance spectra of the bRC of *Rb. sphaeroides*. All of these values are in qualitative agreement with the present calculations. The somewhat smaller values reported for room temperature probably reflect a thermally induced dephasing of the mixed exciton/CT state.[59]

B. Short-Range Coupling Creates an Energy Sink in the Special Pairs. The photosystem of purple bacteria consists of a ring-shaped LH1 core antenna surrounding the reaction center and peripheral ring-shaped LH2 complexes.[60] An excitation energy funnel is created in these complexes between a ring of weakly coupled BChl's and a ring of strongly coupled BChl's that absorb at 800 and 850 nm, respectively, in LH2 and the larger number of strongly interacting BChl*a* molecules in the LH1 ring that absorbs around 875 nm. In order to trap the excitation energy efficiently in the reaction center, the primary electron donor should absorb at an energy that is lower or at least not much higher than the absorption maximum of the LH1 ring. The low-energy absorbance band of the bRC is at 890 nm at 15 K and increases in energy to 860 nm at room temperature,[50] a shift that was explained recently by a dynamic localization of a mixed exciton/CT state.[59] The monomeric BChl*a* molecules in bRC absorb around 800 nm and would therefore be inefficient traps for the excitation energy of LH1. It seems that nature has used the short-range interaction in the special pair to create a sink for excitation energy.[20] If one takes the 800 nm absorption of the monomeric BChl*a* as the value of the wavelength, at which the special pair would absorb without the pigment−pigment coupling, the shift to 890 nm corresponds to an energy shift of 1260 cm^{-1}.

We note that, due to the coupling to the CT states, the low-energy exciton state couples stronger to the low-frequency vibrations than a monomeric state. A reorganization energy of 230 cm^{-1} of this coupling was reported[61,62] for the dimer state, whereas that of a monomeric state in a protein environment is typically in the order of ≈50−100 cm^{-1}.[63,64] Since our quantum chemical calculations were performed in vacuum, they do not include this reorganization energy. The experimental difference in absorption maxima corresponds to a shift of 1440 cm^{-1} of the zero−zero transition energies taking into account the above reorganization energies. This value can be directly compared with the calculated average difference $(\varepsilon_1^{(0)} + \varepsilon_2^{(0)})/2 - E_-$ of 1642 cm^{-1}, which is in good qualitative agreement.

As seen in Figure 8, the major part of the site energy shift is due to the short-range interaction, which also dominates the excitonic coupling (Table 1). We note that, besides shortcomings of the quantum chemical methods and the effective two-state model, the above deviations between calculations and experiment are very likely due to long-range electrostatic effects of the protein on the site energies, which were neglected here. We have recently developed a method for the calculation of these effects.[65] The successful application of this method to the FMO protein shows that protein induced site energy shifts of up to 300 cm^{-1} can well be expected.

The reaction center of PSI is surrounded by a large core antenna system that contains 90 Chl*a* pigments,[29] which are arranged in a much less ordered way as the pigments in the LH1 core antenna of purple bacteria. Some of the antenna Chl's in PSI are so close to each other that short-range effects of the pigment−pigment coupling are believed to shift their absorption maximum to very long wavelengths, depending on the species.[66−69] The red-most band of the PSI core antenna of *T. elongatus* absorbs around 720 nm.[69] At present, the physiological importance of these so-called red Chl's is not clear. At room temperature, the thermal energy is large enough to allow for an efficient trapping of excitation energy by the reaction center.

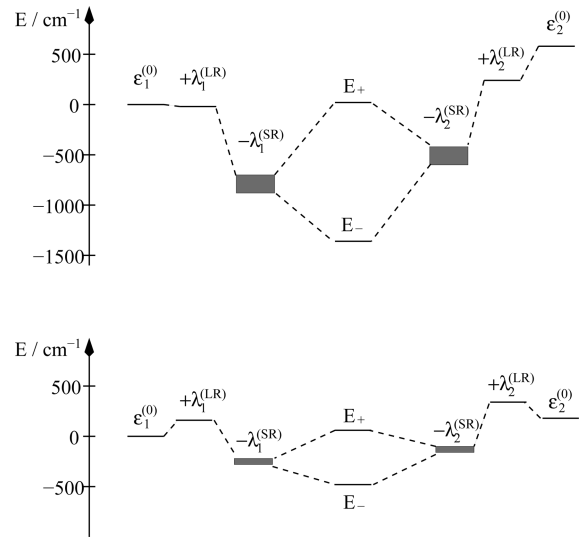

Figure 8. Shift of energy levels by short- and long-range intermolecular couplings in the special pairs of bRC (top) and PSI (bottom), obtained with HF/CIS and TDDFT/BHHLYP, respectively (Tables 1 and 2). The gray squares illustrate the error margins of short-range site energy shifts.

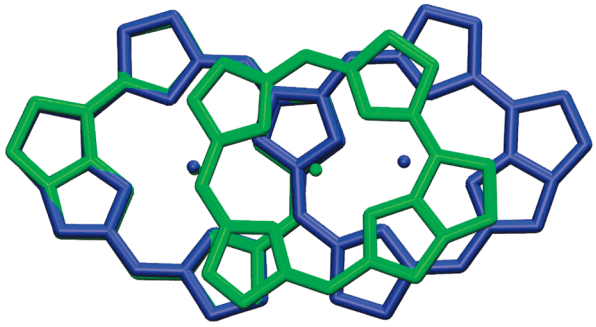

Figure 9. Overlay of the tetrapyrrole skeleton of the special pairs of bRC of *Rb. sphaeroides*[28] (blue) and PSI of *T. elongatus*[29] (green) viewed from above the π-planes. The overlay was obtained from a minimization of the mean-square deviation in positions of equivalent atoms of one dimer half of the two molecule pairs using the program VMD.[74]

Therefore, one possible functional role of the red Chl's would be an increase of the absorption cross section of the reaction center for long-wavelength light.[70]

The low-energy exciton state of the special pair in PSI absorbs around 700 nm[71] and is therefore called P700. Persistent nonphotochemical hole burning studies showed that, as in bRC, the special pair in PSI couples strongly to low-frequency vibrations, with a reorganization energy of about 200 cm^{-1},[62,72] reflecting the CT character of this state. Taking into account an average excitation energy of a monomeric Chl in PSI corresponding to 676 nm[31] and a corresponding reorganization energy of 50 cm^{-1}, the experimental shift in zero−zero transition energy of the special pair is estimated to be ≈650 cm^{-1}, which is close to the average shift $(\varepsilon_1^{(0)} + \varepsilon_2^{(0)})/2 - E_-$ of 570 cm^{-1} estimated from the present calculations.

The close similarity of the special pair structures in bRC and PSI raises the question of why the short-range effects in bRC are stronger. One might even expect the opposite, since the center-to-center distance is smaller by 1.9 Å for the special pair in PSI. As seen in Figure 9, the mode of π-stacking is different in the two dimers. In the bRC, the tetrapyrrole macrocycles are in an eclipsed conformation that guarantees maximal intermolecular overlap of p-orbitals of ring A and one methine bridge. In contrast, the conformation in PSI is more staggered, causing a decrease of orbital overlap despite the shorter center-to-center distance between the two pigments. This change in dimer geometry not only causes a decrease of electron exchange between the dimer halves in PSI compared to bRC but also changes the intermolecular Coulomb interactions. The latter effect leads to a different direction of the long-range site energy shifts in the two reaction centers. Both effects make the excitation energy trap in PSI shallower than that in bRC by about a factor of 3.

In both reaction centers, the short-range interactions are responsible for the creation of an excitation energy sink. Whereas there is no doubt about the special pair in bRC to be the primary electron donor, a discussion about the identity of this donor has started for PSI.[73] The present calculations show that, also in PSI, the short-range interaction shifts the low-energy states of the special pair significantly with respect to the other pigments. The red-shift of the special pair in the reaction center might be needed for efficient harvesting of low-energy light quanta from the red Chl's. This excitation energy transfer could occur directly or indirectly via superexchange or thermally activated transfer through intermediate high-energy antenna states. We have performed similar dimer calculations on all neighboring pigments in the reaction center of PSI and find significant short-range effects only between the two special pair pigments. The magnitude of the short-range effects in the special pair is larger than typical long-range effects on the site energies[65] and also larger than the excitonic coupling between the special pair pigments and the remaining reaction center pigments. Therefore, the low-energy exciton state of the reaction center is dominated by the two special pair pigments. Hence, the most straightforward conclusion is that, also in PSI, primary electron transfer starts at the special pair.

C. Mono- versus Biexponential Distance Dependencies of Short-Range Excitonic Coupling and Site Energy Shifts. To obtain a qualitative understanding of why the distance dependence of the short-range excitonic coupling V_{SR} is monoexponential and that of the short-range site energy shift $\lambda_i^{(SR)}$ is biexponential, we consider a perturbation theory in the coupling between the local excited states $|\Psi_1\rangle$ and $|\Psi_2\rangle$ and two local CT states $|\Psi_3\rangle$ and $|\Psi_4\rangle$. Using the Hamiltonian $\mathbf{H_4}$ in eq A1 of Appendix A, within second-order perturbation theory, the following short-range site energy shift $\lambda_i^{(SR)}$ is obtained for the two local excited states

$$\lambda_1^{(SR)} \approx \frac{(V_{ET})^2}{\varepsilon_3 - \varepsilon_1} + \frac{(V_{HT})^2}{\varepsilon_4 - \varepsilon_1}$$
$$\lambda_2^{(SR)} \approx \frac{(V_{HT})^2}{\varepsilon_3 - \varepsilon_2} + \frac{(V_{ET})^2}{\varepsilon_4 - \varepsilon_2} \qquad (23)$$

Assuming an exponential distance dependence of the matrix elements for electron transfer and hole transfer, i.e., $V_{ET} \propto \exp(-\beta_{ET}\Delta r)$ and $V_{HT} \propto \exp(-\beta_{HT}\Delta r)$, the above site energy shifts should depend biexponentially on distance, if $\beta_{ET} \neq \beta_{HT}$, i.e.,

$$\lambda_i^{(SR)} \propto f_i e^{-2\beta_{ET}\Delta r} + g_i e^{-2\beta_{HT}\Delta r} \qquad (24)$$

Here, the two constants f_i and g_i depend on the inverse energy differences between the states according to eq 23.

In order to obtain an estimate for the short-range excitonic coupling V_{SR}, we consider the mixed local excited/CT state $|\tilde{\Psi}_1\rangle$

$= a|\Psi_1\rangle + \alpha_3|\Psi_3\rangle + \alpha_4|\Psi_4\rangle$ (see eq 2). Within first-order perturbation theory in V_{ET} and V_{HT}, the coefficients α_3 and α_4 are obtained as

$$\alpha_3 \approx \frac{V_{ET}}{\varepsilon_1 - \varepsilon_3} \qquad \alpha_4 \approx \frac{V_{HT}}{\varepsilon_1 - \varepsilon_4} \tag{25}$$

The effective interaction $\tilde{V}$ between the local excited states can then be written as

$$\langle\tilde{\Psi}_1|\hat{V}|\Psi_2\rangle = N_1^{-1}(a\langle\Psi_1|\hat{V}|\Psi_2\rangle + \alpha_3\langle\Psi_3|\hat{V}|\Psi_2\rangle + \alpha_4\langle\Psi_4|\hat{V}|\Psi_2\rangle) \tag{26}$$

where the operator $\hat{V}$ represents the intermolecular coupling. If we neglect the contribution of Dexter exchange contained in $\langle\Psi_1|\hat{V}|\Psi_2\rangle$, we get from eqs 25 and 26 a perturbative approximation for the short-range coupling due to CT states:

$$V_{SR} \approx N_1^{-1}(\alpha_3 V_{HT} + \alpha_4 V_{ET}) = h_{12}e^{-(\beta_{ET}+\beta_{HT})\Delta r} \tag{27}$$

with $h_{12} = N_1^{-1}((\varepsilon_1 - \varepsilon_3)^{-1} + (\varepsilon_1 - \varepsilon_4)^{-1})$.

From a comparison of eqs 24 and 27, it is seen that a biexponential distance dependence of $\lambda_i^{(SR)}$ and a monoexponential distance dependence of V_{SR} is expected in the present perturbation theory limit for $\beta_{ET} \neq \beta_{HT}$. If, for example, we assume $\beta_{ET} > \beta_{HT}$, we get $\beta_{ET} = 1.4$ Å^{-1} and $\beta_{HT} = 0.2-0.4$ Å^{-1} from the fit parameters in Tables 3 and 4. That is, we have $\beta_{ET} + \beta_{HT} = 1.6-1.8$ Å^{-1}, which contrasts with the $\beta_{ET} + \beta_{HT} = 2.8$ Å^{-1} obtained from eq 27 and the distance dependence of V_{SR} (Figure 5).

If $\beta_{ET} \approx \beta_{HT}$, we would expect a monoexponential distance dependence with the same exponent $2\beta_{ET} = 2\beta_{HT}$ for V_{SR} and $\lambda_i^{(SR)}$. In fact, the large exponent obtained for $\lambda_i^{(SR)}$ agrees with the $\beta = 2.8$ Å^{-1} obtained for V_{SR}. We, therefore, conclude that $\beta_{ET} \approx \beta_{HT} \approx 1.4$ Å^{-1}, and that the second attenuation factor of the distance dependence of the site energy shift has an origin other than electron or hole transfer. A likely candidate is the dispersive interaction between π-electron clouds, that is not explicitly taken into account in the four-state Hamiltonian $\mathbf{H_4}$ but is of course present in the quantum chemical dimer calculations.

VI. Conclusions

We have presented a method to calculate the influence of short-range intermolecular interactions in molecular dimers on the excitonic coupling and the local transition energies. These quantities can be directly incorporated into standard exciton Hamiltonians used to study optical properties of dye aggregates. Two important features of the present method are that it allows one to take into account asymmetric site energy shifts and that it provides a consistency check of the effective two-state approach and the quantum chemical method. This check and the comparison of the extracted quantities with parameters fitted in the literature from modeling of optical spectra are used to evaluate the performance of different quantum chemical methods. The latter differ by the relative amount of exact exchange and dynamical electron correlation that is taken into account. The known deficiency of TDDFT in describing CT state energies for vanishing wave function overlap does not influence the present results, since the CT states only enter via a superexchange mechanism. The applications so far suggest that an eclipsed intermolecular configuration of π-electron clouds requires inclusion of more exact exchange than a more staggered configuration.

Application to dimers of BChl and Chl known as the special pairs of the bRC of *Rb. sphaeroides* and PSI of *T. elongatus*, respectively, revealed that the excitonic coupling is almost entirely determined by short-range effects decreasing exponentially with interplane distance and an attenuation factor of $\beta = 2.8$ Å^{-1}. In both special pairs, a significant additional red-shift of the low- and high-energy exciton states occurs due to short-range effects on the local transition energies of the monomers. This shift amounts to about twice the excitonic coupling. Both effects together create excitation energy sinks in these special pairs. In the case of bRC, such a trap is needed to allow for efficient energy transfer from the core light-harvesting complex that has a red-shifted absorbance (and emission) due to predominantly long-range excitonic couplings. In the case of PSI, we argue the red-shift of the special pair is needed to allow for an efficient harvesting of low-energy photons collected by the red Chl's in the core antenna. The latter probably have red-shifted absorption spectra due to short-range effects as well. We identify the excitation energy sink in the reaction center of PSI with the special pair.

Appendix A

Four-State Hamiltonian with Charge-Transfer States. We start from a four-state description of the molecular dimer, in which we consider the two localized excited states $|\Psi_1\rangle = |D^*A\rangle$ and $|\Psi_2\rangle = |DA^*\rangle$ and the two CT states $|\Psi_3\rangle = |D^+A^-\rangle$ and $|\Psi_4\rangle = |D^-A^+\rangle$ corresponding to a one-electron transfer from either D to A or *vice versa*. If we denote the energies of these four states with respect to the energy of the electronic ground state of the dimer, $|\Psi_0\rangle = |DA\rangle$, with $\varepsilon_1, \ldots, \varepsilon_4$, the four-state Hamiltonian $\mathbf{H_4}$ reads

$$\mathbf{H_4} = \begin{pmatrix} \varepsilon_1 & V_{ex} & V_{ET} & V_{HT} \\ V_{ex} & \varepsilon_2 & V_{HT} & V_{ET} \\ V_{ET} & V_{HT} & \varepsilon_3 & V_{CT} \\ V_{HT} & V_{ET} & V_{CT} & \varepsilon_4 \end{pmatrix} \tag{A1}$$

The off-diagonal elements are motivated by the Hartree−Fock approximation sketched in the Supporting Information, where $V_{ex} = K_{ex} + J_{ex}$, V_{ET}, V_{HT}, and V_{CT} are, respectively, the matrix elements of Förster- and Dexter-type excitonic coupling between the two localized excited states, electron transfer between LUMOs, hole transfer between HOMOs, and combined electron and hole transfer connecting directly the two CT states. The eigenstates of $\mathbf{H_4}$ have energies $E_1, \ldots, E_4$, where E_1 and E_2 are the energies of the (delocalized) exciton states (linear combinations of local excited states) of the dimer with some admixture of the two CT states and $E_3, E_4 \gg E_1, E_2$ are the energies of the two linear combinations of the CT states with some admixture of the two local excited states.

Appendix B

Diagonalization of Effective Two-State Hamiltonian and Extraction of Short-Range Quantities. The Hamiltonian in eq 1 is diagonalized with the help of the transformation

$$\begin{pmatrix} E_- & 0 \\ 0 & E_+ \end{pmatrix} = \begin{pmatrix} -u & s \\ s & u \end{pmatrix} \begin{pmatrix} \theta_1 - \lambda_1^{(SR)} & \tilde{V} \\ \tilde{V} & \theta_2 - \lambda_2^{(SR)} \end{pmatrix} \begin{pmatrix} -u & s \\ s & u \end{pmatrix} \tag{B1}$$

where

$$\theta_i = \varepsilon_i^{(0)} + \lambda_i^{(LR)} \tag{B2}$$

The eigenstates $|\Psi_+\rangle$ and $|\Psi_-\rangle$ are obtained as

$$|\Psi_+\rangle = s|\tilde{\Psi}_1\rangle + u|\tilde{\Psi}_2\rangle \tag{B3}$$

$$|\Psi_-\rangle = -u|\tilde{\Psi}_1\rangle + s|\tilde{\Psi}_2\rangle \tag{B4}$$

with energies $E_\pm = {}^1/_2(\theta_1 + \theta_2 - \lambda_1^{(SR)} - \lambda_2^{(SR)}) \pm |\tilde{V}|(\kappa^2 + 1)^{1/2}$, where we introduced the following parameters: $\kappa = (\theta_2 - \theta_1 + \lambda_1^{(SR)} - \lambda_2^{(SR)})/2\tilde{V}$, $s = 1/(1 + Y^2)^{1/2}$, $u = Y/(1 + Y^2)^{1/2}$

$$Y = \frac{u}{s} = \kappa + \frac{\tilde{V}}{|\tilde{V}|}\sqrt{\kappa^2 + 1} \tag{B5}$$

Note that $E_+ > E_-$ in our notation. From these equations, we obtain eqs 6 and 7 in the main text.

To determine Y, we consider the transition dipole moments $\boldsymbol{\mu}_{\mathbf{0}\pm} = \langle\Psi_0|\hat{\mu}|\Psi_\pm\rangle$ of the transition between the ground state $|\Psi_0\rangle$ and the exciton states $|\Psi_\pm\rangle$

$$\boldsymbol{\mu}_{\mathbf{0}+} = s\tilde{\boldsymbol{\mu}}_{01} + u\tilde{\boldsymbol{\mu}}_{02} \tag{B6}$$

$$\boldsymbol{\mu}_{\mathbf{0}-} = -u\tilde{\boldsymbol{\mu}}_{01} + s\tilde{\boldsymbol{\mu}}_{02} \tag{B7}$$

where $\tilde{\boldsymbol{\mu}}_{01/2} = \langle\Psi_0|\hat{\mu}|\tilde{\Psi}_{1/2}\rangle$ are the transition dipole moments of the states $|\tilde{\Psi}_{1/2}\rangle$. If we assume that the CT states $|\tilde{\Psi}_k\rangle$ in eqs 2 and 3 are dark, i.e., have zero transition dipole moments, we obtain

$$\boldsymbol{\mu}_{\mathbf{0}+} = sa'\boldsymbol{\mu}_{01} + ub'\boldsymbol{\mu}_{02} \tag{B8}$$

$$\boldsymbol{\mu}_{\mathbf{0}-} = -ua'\boldsymbol{\mu}_{01} + sb'\boldsymbol{\mu}_{02} \tag{B9}$$

with $a' = aN_1^{-1}$ and $b' = bN_2^{-1}$. From the above equations, we get

$$sa' = \frac{(\boldsymbol{\mu}_{0+}\cdot\boldsymbol{\mu}_{01})(\boldsymbol{\mu}_{02})^2 - (\boldsymbol{\mu}_{0+}\cdot\boldsymbol{\mu}_{02})(\boldsymbol{\mu}_{01}\cdot\boldsymbol{\mu}_{02})}{(\boldsymbol{\mu}_{01})^2(\boldsymbol{\mu}_{02})^2 - (\boldsymbol{\mu}_{01}\cdot\boldsymbol{\mu}_{02})^2} \tag{B10}$$

$$ub' = \frac{(\boldsymbol{\mu}_{0+}\cdot\boldsymbol{\mu}_{02})(\boldsymbol{\mu}_{01})^2 - (\boldsymbol{\mu}_{0+}\cdot\boldsymbol{\mu}_{01})(\boldsymbol{\mu}_{01}\cdot\boldsymbol{\mu}_{02})}{(\boldsymbol{\mu}_{01})^2(\boldsymbol{\mu}_{02})^2 - (\boldsymbol{\mu}_{01}\cdot\boldsymbol{\mu}_{02})^2} \tag{B11}$$

$$ua' = -\frac{(\boldsymbol{\mu}_{0-}\cdot\boldsymbol{\mu}_{01})(\boldsymbol{\mu}_{02})^2 - (\boldsymbol{\mu}_{0-}\cdot\boldsymbol{\mu}_{02})(\boldsymbol{\mu}_{01}\cdot\boldsymbol{\mu}_{02})}{(\boldsymbol{\mu}_{01})^2(\boldsymbol{\mu}_{02})^2 - (\boldsymbol{\mu}_{01}\cdot\boldsymbol{\mu}_{02})^2} \tag{B12}$$

$$sb' = \frac{(\boldsymbol{\mu}_{0-}\cdot\boldsymbol{\mu}_{02})(\boldsymbol{\mu}_{01})^2 - (\boldsymbol{\mu}_{0-}\cdot\boldsymbol{\mu}_{01})(\boldsymbol{\mu}_{01}\cdot\boldsymbol{\mu}_{02})}{(\boldsymbol{\mu}_{01})^2(\boldsymbol{\mu}_{02})^2 - (\boldsymbol{\mu}_{01}\cdot\boldsymbol{\mu}_{02})^2} \tag{B13}$$

Hence, the Y in eq B5 can be obtained either from eqs B10 and B12

$$Y = \frac{ua'}{sa'} = Y_a \tag{B14}$$

or from eqs B11 and B13

$$Y = \frac{ub'}{sb'} = Y_b \tag{B15}$$

In order to avoid unphysical solutions, it is necessary to check whether sa' and sb' are positive. The s is positive by definition (see above). A negative a' or b' would be in conflict with the definition of states $|\tilde{\Psi}_1\rangle$ and $|\tilde{\Psi}_2\rangle$ in eqs 2 and 3. If the calculations based on eqs B10−B13 yield a negative sa' (sb'), the transition dipole moment $\boldsymbol{\mu}_{0+}$ ($\boldsymbol{\mu}_{0-}$) has to be rotated by 180°. Such a rotation is allowed, because the transition density is only determined up to a factor of ±1. A rotation of one of the two transition dipole moments results in a sign change of Y_a and Y_b, whereas rotating both transition dipole moments leaves Y_a and Y_b unchanged. Therefore, it holds that Y_a and Y_b switch sign only if $sa'sb' < 0$. This condition is expressed by the factor f in eq 12.

Appendix C

Explanation for eq 20. If $(1 - |Y_a|)(1 - |Y_b|) < 0$, i.e., the absolute value of one solution for $Y = u/s$ is larger than 1 and the second is smaller than 1, the character of the wave functions $|\tilde{\psi}_1\rangle$ and $|\tilde{\psi}_2\rangle$ is different for the two solutions, as illustrated in Figure 10 for the case $|Y_a| < 1$, $|Y_b| > 1$. For $|Y| < 1$, $|\tilde{\psi}_1\rangle$ is closer in energy to $|\psi_+\rangle$, whereas, for $|Y| > 1$, $|\tilde{\psi}_1\rangle$ is closer in energy to $|\psi_-\rangle$. It holds that (Figure 10)

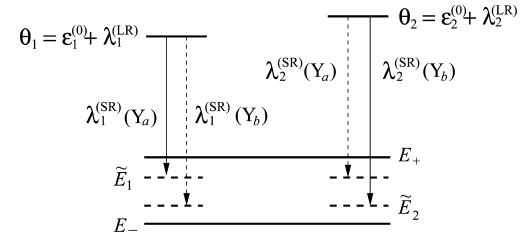

Figure 10. Schematic representation of the existence of two solutions that differ in the relative weight of the two monomers in the exciton states of the dimer.

$$\lambda_2^{(SR)}(Y_b) = \lambda_1^{(SR)}(Y_a) + \theta_2 - \theta_1 \quad \text{(C1)}$$

and

$$\lambda_2^{(SR)}(Y_a) = \lambda_1^{(SR)}(Y_b) + \theta_2 - \theta_1 \quad \text{(C2)}$$

These equations are taken into account in the error estimate in eq 20.

Acknowledgment. We thank N. Krauβ for providing corrected crystal structure data of PSI. T.R. and M.E.-A.M. acknowledge support from the Cluster of Excellence "Unifying Concepts in Catalysis" coordinated by the Technische Universität Berlin and funded by the Deutsche Forschungsgemeinschaft.

Supporting Information Available: Motivation of the four-state Hamiltonian in Appendix A, discussion of the overlap problem in the diagonalization of the effective two-state Hamiltonian, distance dependence of long-range site energy shifts, and coordinates of Chla'. This material is available free of charge via the Internet at http://pubs.acs.org.

References and Notes

(1) Nelson, N.; Ben-Shem, A. *Nat. Rev. Mol. Cell Biol.* **2004**, *5*, 971.
(2) Blankenship, R. E. *Molecular Mechanisms of Photosynthesis*; Blackwell Science: Oxford, U.K., 2002.
(3) Renger, G., Ed. *Primary Processes of Photosynthesis, Principles and Apparatus*; Royal Society Chemistry: Cambridge, U.K., 2008.
(4) Green, B. R., Parson, W. W. Eds. *Light-Harvesting Antennas in Photosynthesis*; Kluwer Academic Publishers: Dordrecht, The Netherlands, 2003.
(5) van Amerongen, H.; Valkunas, L.; van Grondelle, R. *Photosynthetic Excitons*; World Scientific: Singapore, 2000.
(6) May, V.; Kühn, O. *Charge and Energy Transfer Dynamics in Molecular Systems: A Theoretical Introduction*; Wiley-VCH: Berlin, Germany, 2000.
(7) Renger, T.; May, V.; Kühn, O. *Phys. Rep.* **2001**, *343*, 137.
(8) Scheer, H., Ed. *Chlorophylls*; CRC Press: Boca Raton, FL, 1991.
(9) Grimm, B., Porra, R. J., Rüdiger, W., Scheer, H., Eds. *Chlorophylls and Bacteriochlorophylls*; Springer: Dordrecht, The Netherlands, 2006.
(10) Zinth, W.; Wachtveitl, J. *ChemPhysChem* **2005**, *6*, 871.
(11) Renger, G.; Renger, T. *Photosynth. Res.* **2008**, *98*, 53.
(12) Golbeck, J. H., Ed. *Photosystem I: The Light-Driven Plastocyanin: Ferredoxin Oxidoreductase*; Springer: Dordrecht, The Netherlands, 2006.
(13) Scholes, G. D. *Annu. Rev. Phys. Chem.* **2003**, *54*, 57.
(14) Madjet, M. E.; Abdurahman, A.; Renger, T. *J. Phys. Chem. B* **2006**, *110*, 17268.
(15) Förster, T. *Ann. Phys.* **1948**, *437*, 55.
(16) Cheng, Y. C.; Fleming, G. R. *Annu. Rev. Phys. Chem.* **2009**, *60*, 241.
(17) Weiss, C., Jr. *J. Mol. Spectrosc.* **1972**, *44*, 37.
(18) Philipson, K. D.; Tsai, S. C.; Sauer, K. *J. Phys. Chem.* **1971**, *75*, 1440.
(19) Chang, J. C. *J. Chem. Phys.* **1977**, *67*, 3901.
(20) Warshel, A.; Parson, W. W. *J. Am. Chem. Soc.* **1987**, *109*, 6143.
(21) Krueger, B. P.; Scholes, G. D.; Fleming, G. R. *J. Phys. Chem. B* **1998**, *102*, 5378.
(22) Dexter, D. L. *J. Chem. Phys.* **1953**, *21*, 836.
(23) Harcourt, R. D.; Scholes, G. D.; Ghiggino, K. P. *J. Chem. Phys.* **1994**, *101*, 10521.
(24) Scholes, G. D.; Ghiggino, K. P. *J. Chem. Phys.* **1994**, *101*, 1251.
(25) Newton, M. D. *Chem. Rev.* **1991**, *91*, 767.
(26) Hsu, C. P. *Acc. Chem. Res.* **2009**, *42*, 509.
(27) Scholes, G. D.; Gould, I. R.; Cogdell, R. J.; Fleming, G. R. *J. Phys. Chem. B* **1999**, *103*, 2543.
(28) Stowell, M. H. B.; McPhillips, T. M.; Soltis, S. M.; Rees, D. C.; Abresch, E.; Feher, G. *Science* **1997**, *276*, 812.
(29) Jordan, P.; Fromme, P.; Witt, H. T.; Klukas, O.; Saenger, W.; Krauss, N. *Nature* **2001**, *411*, 909.
(30) Won, Y.; Friesner, R. A. *J. Phys. Chem.* **1988**, *92*, 2208.
(31) Byrdin, M.; Jordan, P.; Krauss, N.; Fromme, P.; Stehlik, D.; Schlodder, E. *Biophys. J.* **2002**, *83*, 433.
(32) Brüggemann, B.; Sznee, K.; Novoderezhkin, V.; van Grondelle, R.; May, V. *J. Phys. Chem. B* **2004**, *108*, 13536.
(33) Jordanides, X. J.; Scholes, G. D.; Fleming, G. R. *J. Phys. Chem. B* **2001**, *105*, 1652.
(34) Knapp, E. W.; Scherer, P. O. J.; Fischer, S. F. *Biochim. Biophys. Acta* **1986**, *852*, 295.
(35) Scherer, P. O. J.; Fischer, S. F. *Biochim. Biophys. Acta* **1987**, *891*, 157.
(36) Mar, T.; Gingras, G. *Biochemistry* **1995**, *34*, 9071.
(37) Knox, R. S.; Spring, B. Q. *Photochem. Photobiol.* **2003**, *77*, 497.
(38) Adolphs, J.; Renger, T. *Biophys. J.* **2006**, *91*, 2778.
(39) Adolphs, J.; Müh, F.; Madjet, M. E.; Renger, T. *Photosynth. Res.* **2008**, *95*, 197. Erratum: **2008**, *95*, 211.
(40) Brooks, B. R.; Bruccoleri, R. E.; Olafson, B. D.; States, D. J.; Swaminathan, S.; Karplus, M. *J. Comput. Chem.* **1983**, *4*, 187.
(41) MacKerell, A. D.; Bashford, D.; Bellott, M.; Dunbrack, R. L.; Evanseck, J. D.; Field, M. J.; Fischer, S.; Gao, J.; Guo, H.; Ha, S.; Joseph-McCarthy, D.; Kuchnir, L.; Kuczera, K.; Lau, F. T. K.; Mattos, C.; Michnick, S.; Ngo, T.; Nguyen, D. T.; Prodhom, B.; Reiher, W. E.; Roux, B.; Schlenkrich, M.; Smith, J. C.; Stote, R.; Straub, J.; Watanabe, M.; Wiorkiewicz-Kuczera, J.; Yin, D.; Karplus, M. *J. Phys. Chem. B* **1998**, *102*, 3586.
(42) *Jaguar 5.5*; Schrödinger, L.L.C.: Portland, OR, 1991−2003.
(43) Kong, J.; White, C. A.; Krylov, A. I.; Sherrill, D.; Adamson, R. D.; Furlani, T. R.; Lee, M. S.; Lee, A. M.; Gwaltney, S. R.; Adams, T. R.; Ochsenfeld, C.; Gilbert, A. T. B.; Kedziora, G. S.; Rassolov, V. A.; Maurice, D. R.; Nair, N.; Shao, Y. H.; Besley, N. A.; Maslen, P. E.; Dombroski, J. P.; Daschel, H.; Zhang, W. M.; Korambath, P. P.; Baker, J.; Byrd, E. F. C.; Van Voorhis, T.; Oumi, M.; Hirata, S.; Hsu, C. P.; Ishikawa, N.; Florian, J.; Warshel, A.; Johnson, B. G.; Gill, P. M. W.; Head-Gordon, M.; Pople, J. A. *J. Comput. Chem.* **2000**, *21*, 1532.
(44) Koch, W.; Holthausen, M. C. *A chemist's guide to density functional theory*; Wiley, VCH: 2001.
(45) Becke, A. D. *Phys. Rev. A* **1988**, *38*, 3098.
(46) Lee, C.; Wang, W.; Parr, R. G. *Phys. Rev. B* **1988**, *37*, 785.
(47) Slater, J. C. *Quantum theory of molecules and solids*; McGraw-Hill: New York, 1974.
(48) Vosko, S. H.; Wilk, L.; Nusair, M. *Can. J. Phys.* **1980**, *58*, 1200.
(49) Sigfridsson, E.; Ryde, U. *J. Comput. Chem.* **1998**, *19*, 377.
(50) Huber, H.; Meyer, M.; Scheer, H.; Zinth, W.; Wachtveitl, J. *Photosynth. Res.* **1998**, *55*, 153.
(51) Rae, M.; Fedorov, A.; Berberan-Santos, M. N. *J. Chem. Phys.* **2003**, *119*, 2223.
(52) Cai, Z.-L.; Crossley, M. J.; Reimers, J. R.; Kobayashi, R.; Amos, R. D. *J. Phys. Chem. B* **2006**, *110*, 15624.
(53) Yanai, T.; Tew, D. P.; Handy, N. C. *Chem. Phys. Lett.* **2004**, *393*, 51.
(54) Dreuw, A.; Head-Gordon, M. *Chem. Rev.* **2005**, *105*, 4009.
(55) Stein, T.; Kronik, L.; Baer, R. *J. Am. Chem. Soc.* **2009**, *131*, 2818.
(56) Lange, A. W.; Rohrdanz, M. A.; Herbert, J. M. *J. Phys. Chem. B* **2008**, *112*, 6304.
(57) Dreuw, A.; Weisman, J. L.; Head-Gordon, M. H. *J. Chem. Phys.* **2003**, *119*, 2943.
(58) Miura, M.; Yuriko, A.; Champagne, B. *J. Chem. Phys.* **2007**, *127*, 084103.
(59) Renger, T. *Phys. Rev. Lett.* **2004**, *93*, 188101.
(60) Law, C. J.; Cogdell R. J. The Light-Harvesting System of Purple Anoxygenic Photosynthetic Bacteria. In *Primary Processes of Photosynthesis - Part I, Principle and Apparatus*; Renger, G., Ed.; RCS Publishing: Cambridge, U.K., 2008; p 205.
(61) Lyle, P. A.; Kolaczkowski, S. V.; Small, G. J. *J. Phys. Chem.* **1993**, *97*, 6924.
(62) Small, G. *J. Chem. Phys.* **1995**, *197*, 239.
(63) Renger, T.; Marcus, R. A. *J. Chem. Phys.* **2002**, *116*, 9997.
(64) Raszewski, G.; Renger, T. *J. Am. Chem. Soc.* **2008**, *130*, 4431.
(65) Müh, F.; Madjet, M. E.; Adolphs, J.; Abdurahman, A.; Rabenstein, B.; Ishikita, H.; Knapp, E. W.; Renger, T. *Proc. Natl. Acad. Sci. U.S.A.* **2007**, *104*, 16862.
(66) Vaitekonis, S.; Trinkunas, G.; Valkunas, L. *Photosynth. Res.* **2005**, *86*, 185.
(67) Hsin, T. M.; Zazubovich, V.; Hayes, J. M.; Small, G. J. *J. Phys. Chem. B* **2004**, *108*, 10515.
(68) Ihalainen, J. A.; Rätsep, M.; Jensen, P. E.; Scheller, H. V.; Croce, R.; Bassi, R.; Korppi-Tommola, J. E. I.; Freiberg, A. *J. Phys. Chem. B* **2003**, *107*, 9086.
(69) Schlodder, E.; Shubin, V. V.; El-Mohsnawy, E.; Roegner, M.; Karapetyan, N. V. *Biochim. Biophys. Acta* **2007**, *1767*, 732.
(70) Gobets, B.; van Grondelle, R. *Biochim. Biophys. Acta* **2001**, *1507*, 80.
(71) Witt, H.; Bordignon, E.; Carbonera, D.; Dekker, J. P.; Karapetyan, N.; Teutloff, C.; Webber, A.; Lubitz, W.; Schlodder, E. *J. Biol. Chem.* **2003**, 46760.
(72) Gillie, J. K.; Lyle, P. A.; Small, G. J.; Golbeck, J. H. *Photosynth. Res.* **1989**, *22*, 233.
(73) Holzwarth, A. R.; Müller, M. G.; Niklas, J.; Lubitz, W. *Biophys. J.* **2006**, *90*, 552.
(74) Humphrey, W. W.; Dalke, A.; Schulten, K. *J. Mol. Graphics* **1996**, *14*, 33.

JP906009J